Shock Densification / Hot Isostatic Pressing of Titanium Aluminide

SHI-SHYAN SHANG and MARC A. MEYERS

Materials Science Program
University of California, San Diego
La Jolla , CA. 92093 , U.S.A.

Abstract

Consolidation of rapidly solidified titanium aluminide powders (Ti_3Al) employing explosive shock pressure followed by hipping was carried out successfully. Shock densification was achieved by using a double tube design in which the flyer tube was explosively accelerated, impacting the powder container. Elemental mixtures of Ti(15wt%) and Al(15wt%) powders were added to intermetallic compound powders (Ti_3Al). HIP was used to chemically induce bonding between Ti_3Al particles. The highly exothermic reactions were activated by hipping at 1000 ^{0}C and enhanced the bonding between the inert intermetallic powders. Compression tests indicated strong bonding between Ti_3Al particles. Well bonded Ti_3Al compacts having an average ultimate compressive strength of 2 GPa and compressive fracture strain of 20 % were produced by this technique. The ultimate tensile strengths, due to the presence of flaws in the microstructure (microcracks, voids) and intergranular fracture observed in the reacted regions, were much lower (~250 MPa).

To appear, Metallurgical Transactions A

I. INTRODUCTION

Titanium aluminide (Ti_3Al) intermetallics have properties which make them desirable candidates for applications in aircraft turbine engines [1-3]. These ordered intermetallic compounds are less dense and stiffer than conventional titanium alloys. However, a main problem with titanium aluminides is their low ductility at room temperature, making them difficult to fabricate and damage-intolerant. Shock consolidation of rapidly solidified Ti_3Al (RSP) powder is a process that has considerable potential. Shock-densification processing is an attractive alternative for RSP materials since long term thermal exposures are not essential for processing. However, it has been widely reported that there remain two unsolved problems in the shock compaction technique [4-6]. One is cracking of the compacts at both the microscopic and macroscopic levels. The other is a lack of uniformity in microstructure and mechanical properties within resulting compacts. At three recent workshops held in the US [7], the Soviet Union [8] , and Japan [9], cracking was identified as a major unresolved problem. These two problems tend to increase with an increase in the shock pressure used. In order to alleviate these two problems, low shock pressures are desirable. The objectives of this investigation were (1) to eliminate or minimize cracks in resulting compacts; and (2) to use the heat generated from exothermic reaction to help consolidation. Thus, RSP Ti_3Al powders are compacted to pressures as low as possible to just ensure densification of the powder. Then, the highly exothermic reactions of elemental powders (Ti and Al) added to the intermetallics will take place during the hipping stage. The heat produced is dissipated on the surfaces of inert powders and the reacted elemental powders act as a cement to enhance bonding between the powders.

II. EXPERIMENTAL PROCEDURES AND SET-UPS

A schematic of the processes of shock densification and of HIP-induced chemical reaction to help consolidation is illustrated in Fig. 1. The Ti_3Al+Ti+Al powders were placed into powder containers to form a cylindrical green compact (267 mm in length and 37 mm in diameter)

with density of 65% of theoretical. For shock densification, the cylindrical axisymmetric double-tube system (Fig. 2) was used in this study. A detailed description of the system is presented elsewhere [10]. Commercially available ANFO (Ammonium Nitrate-Fuel Oil), modified to produce a lower detonation velocity, was used as the explosive. The detonation velocity was approximately equal to 2200 m/s. The explosive charge is contained in a PVC plastic tube resting on a wood base and surrounds a mild steel flyer tube, in the center of which is the assembly containing the powder (stainless steel pipe with top and bottom steel plugs). The containers are filled with the powder under argon atmosphere. This technique generates pressures in the powder that can be several times higher than the ones generated without flyer tube. The main advantage of this technique is that it allows the use of low detonation velocity explosives for consolidating hard powders, in order to minimize the cracking effects. The explosive was initiated at the top and caused the implosion of the tube containing the powder, as the detonation front ran downward. Well densified Ti_3Al+Ti+Al compacts were obtained (~ 95-98 % of the crystal density) and machined for subsequent hipping and annealing. The density distribution is uniform from top to bottom of the compact. Hot isostatic pressing (HIP) was conducted at Degussa Electronics Inc. at 600 ^{0}C and 1000 ^{0}C. The pressure , 200 MPa , was used for one hour. Specimens were also encapsulated in quartz under vacuum and annealed to different temperatures, ranging from 600 ^{0}C to 1000 ^{0}C. Both original and consolidated compacts were characterized by optical and scanning electron microscopy, X-ray diffraction, microhardness, tensile and compression tests. Compression tests were carried out in the MTS 810 testing machine at a strain rate of 3.5×10^{-4} s^{-1}. The specimens were cylindrical, with a diameter of 6mm and a length of 12mm. Tensile tests were performed at ambient temperature in an INSTRON testing machine with INTERLAKEN computerized controller. Specimens were cut from transverse section of the cylinder. The dimensions of the specimens were: 30 mm length, 10 mm external width, 4 mm internal (gage) width and 1.5 mm thickness.

III. RESULTS AND DISCUSSION

A. *MATERIAL CHARACTERIZATION*

The sizes, shapes, and purities of powders for the experiments are listed in Table 1. The composition of these powders is actually quite different from stoichiometric Ti_3Al: Ti-21wt%Nb- 14wt%Al- 1wt%Er. The powder particles are shown in Fig. 3. Fig. 3(a) shows that the morphology of the Ti-Al-Nb powder is almost perfectly spherical. The Ti-Al-Nb powders were produced through rapid solidification processing (RSP) and were supplied by United Technologies Government Products Division. In rapidly solidified Ti-Al-Nb alloys, the high temperature phase can be quenched to room temperature under sufficient cooling rate [11]. However, the β phase transforms to martensite (α') which can eventually transform to the ordered α_2 phase [12]. Addition of β-stabilizing elements, such as niobium, depresses the M_S temperature. Figs. 3(b) and 3(c) show the titanium and aluminum powders, respectively. Titanium powders are uniform alphabet sized and shaped. Aluminum powders are irregularly shaped. The etched cross-section of the original Ti-Al-Nb powder reveals a microcellular structure (Fig. 4). Fine round white precipitates uniformly decorating the cell are also observed. These precipitates are Er_2O_3 [13,14]. Minor additions of Er_2O_3 particles were made to obtain a homogeneous distribution of fine grains in the matrix. This resulted in an increase in the room temperature strength as well as high temperature creep resistance. The Ti-Al-Nb alloys strengthened by erbia (Er_2O_3) have been the object of considerable study.

B. *SHOCK DENSIFICATION EXPERIMENTS WITH CYLINDRICAL GEOMETRY*

Prummer [18] showed that the degree of densification depends on the detonation pressure of the explosive used for compaction, that is related to the detonation velocity by the following expression :

$$P \approx 2.5\, \rho U_d^2$$

The explosive Chapman-Jouguet pressure P is directly proportional to the square of the detonation velocity U_d , where ρ is the explosive density (kg/m^3). From the Gurney energy of explosive one calculates the impact velocity of the flyer tube, which then provides the pressure in the porous medium. Details of procedure are given by Meyers and Wang [10]. Earlier work by Ferreira et al. [13,14] showed that excessive detonation pressure produces overcompaction (excessive melting) and results in flaws and cracks. The use of a high detonation-velocity explosive ($U_d \sim$ 6000-7000 m/s) resulted in pressures that were excessive. Thus, a low detonation velocity (2200 m/s) for Ti_3Al+Ti+Al was chosen in order to minimize cracking. Successful densification was obtained using this explosive with low detonation velocity, as compared to the compacts produced using explosive with higher detonation velocity (3500 to 6000 m/s). The macrocrack density was reduced by approximately 40%, where macrocrack density was defined as macrocrack surface area per unit volume. This crack density was measured along longitudinal and transverse sections of the specimens at a magnification of 1-5X. The crack length was calculated by the linear intersect method with a grid of perpendicular lines. Greater details are given by Ferreira et al. [13]. The shock pressure was calculated to be 9.5 GPa at a detonation velocity of 2200 m/s. SEM analysis (Fig. 5) of recovered compacts revealed that Ti and Al particles underwent a considerable amount of deformation and that the material was fully densified.The Ti_3Al particles seem to retain their initial sphericity. The Ti_3Al particles exhibited considerably less deformation than the Ti and Al particles during shock densification because of their much higher strength. Since the initial density of Ti_3Al+Ti+Al was around 65% of TD, one can see that the addition of Al and Ti could, upon densification, totally fill the 35% voids existing in the Ti_3Al matrix without need for significant plastic deformation in these Ti_3Al particles. Ti and Al X-ray dot mappings [Figs. 5(a), 5(b)] were performed in order to identify unreacted regions. The white irregular particulates correspond to unreacted Ti and the dark irregular particulates correspond to unreacted Al, while the small grey areas in the image correspond to the reaction products of Ti and Al. These show particles that were subjected to shock

densification with weak bonding. (insufficient pressure for jetting and melting between particles and for extensive reaction). The interior of Ti_3Al particle still retains microcellular structure. Transmission electron microscopy (TEM) revealed the substructural features of the shock-densified alloys. Figs. 6(a) and 6(b) show fine grain size (approximately 500 nm) and dislocations in high densities that are typical of shocked materials. This region is characteristic of the interiors of the Ti_3Al powders. Er_2O_3 dispersoids are clearly seen. Their size and spacing is such that they are effective high temperature strengtheners. There seems to be a tendency for them to arrange themselves in rows (along original Ti_3Al cell boundaries ; see Fig. 4 and 10(b), where arrows identify the rows).

C. *CHEMICALLY-INDUCED ANNEALING AND HOT ISOSTATIC CONSOLIDATION OF Ti_3Al*

The shock densified Ti_3Al compacts were annealed to different temperatures ranging from 600 to 1000 ^{0}C. The unreacted regions (Ti+Al) and porosities were observed in specimens at different temperatures (Fig. 7). These porosities were due to either (a) shrinkage that occurs when Ti and Al reacted; or (b) trapped gases causing expansion of voids. The density of Ti_3Al is 4.2 g/cm^3, while that of Ti and Al are 4.5 and 2.7 g/cm^3, respectively. Thus, the reaction leads to a 25% shrinkage. Since the capsules were not evacuated prior to shock densification, there is trapped air in them. Thus, when the reactants melt, the entrapped gases would expand and form spherical voids, which minimize the surface area. Consequently, hot isostatic pressing (HIP) was conducted at 600 ^{0}C and 1000 ^{0}C for one hour. SEM analysis of the material recovered from hipping at 600 ^{0}C revealed that Ti and Al powders reacted with each other [Fig. 8(a)]. The dark regions correspond to the voids (marked in figure) and the greyish regions (marked in figure) correspond to the reaction products of Ti and Al. Analysis of the material recovered after hipping at 1000 ^{0}C [Fig. 8(b)] revealed that the reaction products bonded the Ti_3Al powders very well, as compared to the compacts produced using hipping at

600 ^{0}C. One can also see the phase separation in the interiors of the particles, after 1000 ^{0}C HIP.

D. *X-RAY ANALYSIS OF Ti_3Al ALLOYS*

In order to determine phase transformation in Ti_3Al particles and the types of reaction products, X-ray diffraction analysis was performed on the original powders and compacts. These results are shown in Fig 9. Comparison of the X-ray peaks for the as-mixed powders [Fig. 9(a)] and for the compacts after the two HIP treatments [Figs. 9(b),(c)] shows phase transformation in the Ti_3Al alloy powder after hipping. In the case of hipping at 600 ^{0}C, the β phase (disordered bcc solid solution) transforms to α_2 (ordered hcp solid solution ; marked H) and orthorhombic phase [Fig. 9(b)]. In the case of hipping at 1000 ^{0}C, the β phase transforms to α_2 , orthorhombic and B2 phase (ordered bcc solid solution) [Fig. 9(c)]. Furthermore, new peaks (TiAl ; marked R) are observed, indicating that reactions (Ti + Al mixture) have occurred during hipping. The present phase transformation results confirm Banerjee et al's observations [15]. They suggested that the orthorhombic phase is derived from the α_2 phase as a result of a phase separation, in which the Ti_3Al phase containing Nb separates into Nb lean and Nb rich regions, and this Nb rich region would transform to the orthorhombic phases. This phase separation reactions are due to Ti_3Al free energy curve inflections with Nb additions. When the free energy vs. composition curve (concave) has a convex region, two inflection points are formed. The region bound by the common tangent will tend to separate into phases. Nb rich regions, closer to the Ti_2NbAl composition, transform to the orthorhombic phase. The stoichiometric composition of the orthorhombic phase corresponds to Ti_2NbAl. Figs. 10(a) and 10(b) show the microstructures of the Ti_3Al particles which were hipped at 600 ^{0}C and 1000 ^{0}C, respectively. Phase transformation (β to α_2) was confirmed in Fig. 10(a). EDS analysis [Fig. 10(b)] revealed that white regions in the particles are Nb rich , and the black regions are Nb lean. These black regions are believed to be α_2 phase, while white regions are believed to be orthorhombic and B2 phases (Nb rich

regions). One can also see stringers of Er_2O_3 dispersions that mark the boundaries of the previous cells.

E. *COMPRESSIVE PROPERTIES OF Ti_3Al ALLOYS*

Table 2 lists the compressive property data for Ti_3Al alloys at room temperature. The data are from shock-densified specimens which were hipped or annealed at various temperatures. The data demonstrate that Ti_3Al exhibits an apparent increase in ductility with increasing temperature of annealing or hipping. The lower ultimate compressive stress and ductility of annealed specimens, compared to the 1000 ^{0}C-hipped specimen, could be due to two reasons: (1) Ti and Al were not totally reacted in annealed specimens (2) shrinkage occurred when Ti and Al reacted, with the production of voids. Hipping at 600 ^{0}C resulted in the α_2 (hcp) and orthorhombic structure and these structures exhibited a high yield stress but low ductility. The fracture surfaces from failed compressive specimens were observed by SEM. The specimen which was hipped at 600 ^{0}C failed by a mixture of shear and axial splitting. Axial splitting (lower portion) is produced by tensile stresses at the tip of the pre-existing cracks and voids due to the compressive forces. Observation of the axial splitting region showed that the individual particles were heavily deformed and exhibited cleavage regions [Fig. 11(a)]. One can observe a microvoid (shown by arrow) , indicating that the failure may have been initiated at these microvoids. This fracture surface is characteristic of brittle materials. Scanning electron micrographs from fractured shear surface (upper part) did not provide any information on the nature of the fracture, because the fracture surface was smeared during shear [Fig. 11(b)]. The failed specimen which was hipped at 1000 ^{0}C had a greater shear component. The ductility of this compact was much higher and microcracks were fewer compared to the 600 ^{0}C-hipped specimen. Fractographs of the 1000 ^{0}C-hipped specimens are the same as Fig. 11(b). Fig. 12(a) shows a crack propagating through the particles; this shows that the bonding of the powders is excellent. Within the particles, the phases shown in Fig. 10 seem to play an important role in crack propagation. At a higher

magnification, one can see intergranular and transgranular cracks in the interior of Ti_3Al particles (Fig. 12(b)). Microcracks form in the α_2 phase (see arrow in Fig. 12(b)) and are arrested (or retarded) by the ductile B2 phase. The B2 phase is a cubic ordered phase that is more ductile than α_2 which is hexagonal. In Fig. 12, one should be careful not misinterpret the main crack surfaces. The whitening is produced by electron charging and enhanced secondary yield. It is not due to a layer of B2. Smaller cracks (marked by arrows) clearly show that the α_2 is the favored path. The black grains which are about 5-10 μm are the α_2 phase. The B2 phase (the white regions) is considered to play an important role in improving the ductility, but the source of the improvement of ductility is not understood. One possibility is that the B2 phase may change the stress field around α_2 matrix, which may affect toughening mechanisms and, consequently, the sample showed higher ductility.

F. *TENSILE PROPERTIES OF Ti_3Al ALLOYS*

Fig. 13 shows the stress vs strain plot in tension for 1000^0C-hipped specimens. The average value of ultimate tensile strength is equal to 250 MPa. In comparison, the average value of ultimate tensile strength for shock consolidated Ti_3Al reported by Ferreira et al. [13] is 59 MPa. The higher tensile properties are due to the reduction of cracks in the 1000^0C-hipped materials. Two different crack morphologies were observed: A cleavage, transgranular fracture mode (from particle interiors) and an intergranular mode (from interparticle regions and particle interiors). The intergranular fracture is shown in Fig. 14. At a higher magnification, precipitates (Er_2O_3) were found at grain boundaries (Fig. 14(b)) and these precipitates originated from the Ti_3Al particles. It is believed that grain boundary embrittlement arises from the thermally activated segregation of impurities along grain boundaries. Impurities at grain boundaries are known to produce loss in cohesion [16]. The grain size of the reacted interparticle region (TiAl) is about 2-3 μm. These grains are indicated by arrows in Fig. 14(b); each arrow indicates one grain. Intergranular and transgranular cracks are observed in the interior regions of Ti_3Al particles (Fig. 15(a)).

Those grains which are 5-10 μm are α_2 phase. The cleavage facets reveal features related to the direction of local crack propagation (Fig. 15(b)).

G. *MICROHARDNESS OF Ti_3Al ALLOYS*

The microhardness of the Ti_3Al powders before and after annealing or hipping was measured to establish the effects of subsequent processing. The microhardness of interparticle melted and resolidified regions was also measured in order to determine whether the interparticle regions had a similar rapidly solidified structure as that of the original powder. A load of 200 gf for 15 seconds was applied to determine the microhardness. The microhardness values of the Ti_3Al particles in as-received condition were determined as 347 ± 17 VHN. Fig. 16 shows the variation of microhardness as a function of processing and temperature. The Ti_3Al particles , after shock densification , have greater microhardness value than the original powders (347 VHN); so , the shock hardening effect is confirmed. As the temperature of processing is raised above 600 ^{0}C , the microhardness of particle interiors decreases in value due to β phase transformation to α_2 and orthorhombic phases, and annealing of the shock-induced substructure. The microhardness of the interparticle region in the hipped material is higher than that of the annealed one. The reason for this difference is the absence of voids in the hipped condition.

IV. CONCLUSIONS

The generic problem with titanium aluminide alloys, as well as most other aluminide based alloys, is their limited ductility and poor toughness at low temperature. Ti_3Al with high ductility (about 20% compressive strain) can be produced by shock densification followed by hipping. This was accomplished by using a low detonation-velocity explosive (2200 m/s detonation velocity) and post-shock HIP. Three main sources of cracking were reduced:

(1)Cracking due to stress-wave propagation, interaction and reflection. By decreasing the amplitudes of compressive shock pulse, the secondary effects are correspondingly decreased.

(2)Thermal stress: Less shock heating is produced at low shock pressures. The annealing/hipping treatments release residual stresses.

(3)Embrittling phase transformation. Previous experiments by Ferreira et al. [13] showed the embrittling phase α_2, while the morphology and distribution of α_2 in the current study was such that the material was more ductile.

Significant differences between compressive and tensile mechanical properties can be seen for the material that underwent hipping at 1000 ^{0}C : the yield stress/UTS in tension is approximately 250 MPa (Fig. 13) ; in contrast, the yield stress (in compression) and ultimate compressive strength are approximately 800 and 1980 MPa, respectively. This eight-fold difference is typical of intermetallics and ceramics and clearly indicates that existing flaws trigger failure in tension. These flaws require much higher stresses to be activated in compression and this also explains the higher ductility in compression than in tension. One can, using a simple model assuming a spherical flaw, show that tensile stresses are generated in compression (see, for example, Ferreira et al. [14]). The differences in compressive and tensile strength can be rationalized in terms of flaw activation [14]. The fracture initiation and propagation is very complex in these alloys and two factors were found to be important: (a) the presence of the α_2 (brittle) and B2 (ductile) phases after hipping, on a fine microstructural scale (~ 5 μm) seems to be a source of ductility (see Fig. 12); (b) weakening of the grain boundaries within the reacted interparticle regions due, perhaps, to segregation of impurities at these boundaries, which is an embrittling effect (see Fig. 14(b)).

ACKNOWLEDGEMENTS

This research was sponsored by the National Science Foundation Materials Processing Initiative Award No. DMR 8713258. The authors would like to thank Dr. Arnaldo Ferreira, Dr. Kenneth Vecchio, Dr. N.N. Thadhani, Mr. Li-Hsing Yu, Dr. Soon-Nam Chang and Mr. Jerry Lasalvia for their assistance during the work. The use of the facilities of the Center of Excellence for Advanced Materials is gratefully acknowledged. The materials were provided

by Ms. S. Shulesko, Pratt and Whitney Government Products Division. The explosive experiment was carried out at EFI, Louisville, Colorado, through the kind assistance of Mr. W. Sharpe.

REFERENCES

1. D. Shechtman, M. J. Blackburn, and H. A. Lipsitt: *Metall. Trans.*, 1974 , vol. 5, pp. 1373-1381

2. H. A. Lipsitt, D. Shechtman, and R. E. Schafrik: *Metall. Trans.* , 1980 , vol. 11A , pp. 1369-1375

3. I. I. Kornilov and T. T. Nartova: *Dokl. Adad, Nauk SSSR.*, 1961 , vol. 114 , p. 829

4. T. Akashi and A. B. Sawaoka: *Adv. Ceram. Mater.*, 1988 , vol. 3 , pp. 288-290

5. S. S. Shang and M. A. Meyers: in "Shock-Wave and High-Strain Rate Phenomena in Materials", eds. M. A. Meyers, L. E. Murr, and K. P. Staudhammer, M. Dekker, 1991, in press

6. K. Hokamoto, S. S. Shang, and M. A. Meyers: in "Shock-Wave and High-Strain Rate Phenomena in Materials", eds. M. A. Meyers, L. E. Murr, and K. P. Staudhammer, M. Dekker, 1991, in press

7. Proc. First Workshop on Industrial Applications of Shock Processing of Powders, CETR , New Mexico Institute of Mining and Technology, Socorro, NM, June 1-3 , 1988.

8. Proc. Seminar on High Energy Rate Working of Rapidly Solidified Materials, Novosibirsk, USSR , 10-14 October , 1988.

9. A. Sawaoka, ed., Proc. Second Workshop on Industrial Applications of Shock Processing of Materials , Tokyo Institute of Technology, Japan, December,1988

10. M. A. Meyers and S. L. Wang: *Acta Metall.* , 1988 , vol. 4 , pp. 925-936

11. E. M. Schulson: *Int. J. Powder Metall.*, 1987 , vol. 23(1) , pp. 25-32

12. M. J. Blackburn: *Trans. Metall. Soc.* , 1967 , vol. 239 , p. 1200

13. A. Ferreira, M. A. Meyers, N. N. Thadhani, S. N. Chang and J. R. Kough: *Metall. Trans.*, 1991, vol. 22 , pp. 685-695

14. A. Ferreira, M. A. Meyers and N. N. Thadhani: *Metall. Trans.* , submitted , 1990.

15. D. Banerjee, A.K. Gogia, T.K. Nandy, and V.A. Joshi: *Acta Metall.* , 1988 , vol. 36 , pp. 871-882

16. R. J. Asaro: *Phil. Trans. R.Soc. Lond.*, 1980 , vol. 295A , pp. 151-163

List of Tables

Table 1 Powder sizes , shapes , and purities of powders

Powder	Size	Source	Shape	Composition
Ti_3Al	65-205 μm	Pratt & Whitney	Spherical	64Ti-21Nb-14Al-1.0Er
Ti	325mesh	CERAC	alphabet	99.5% pure
Al	325mesh	CERAC	Irregular	99.8% pure

Table 2 Mechanical properties for compacted Ti_3Al+Ti+Al powder alloy

No	Treatment	0.2% Yield Strength (MPa)	Ultimate Compressive Strength (MPa)	Fracture Stress in Compression (MPa)	Maximum Compressive Strain (%)
1	As shocked	983	1363	1228	4.50
2	Hip at 600 °C	1081	1579	1317	7.80
3	Anneal at 600 °C	1060	1785	1535	12.68
4	Anneal at 700 °C	997	1745	1407	12.90
5	Anneal at 800 °C	956	1707	1505	12.38
6	Anneal at 1000 °C	819	1958	1495	16.41
7	Hip at 1000 °C	813	1982	1673	20.38

List of Figures

FIG. 11 Fractographs from fractured surface of the 600 ^{0}C hipped specimens in compressive test : (a) lower portion which exhibited cleavage regions (b) upper portion which surfaces were smeared during shear.

FIG. 12 Scanning electron micrograph showing (a) transparticle cracks after compression test (b) intergranular and transgranular cracks in the interior of Ti_3Al particle.

FIG. 13 Stress vs strain curve in tension for specimens after 1000 ^{0}C hipping (results of two tests).

FIG. 14 Fractographs from fractured surface after tensile test showing (a) intergranular cracks in the interparticle region (b) presence of dispersoids (Er_2O_3) at grain boundaries.

FIG. 15 Scanning electron micrograph showing (a) intergranular and transgranular cracks in the Ti_3Al particle after tensile test (b) transgranular cleavage in Ti_3Al particle.

FIG. 16 Microhardness values of Ti_3Al hipped or annealed from 600 ^{0}C to 1000 ^{0}C.

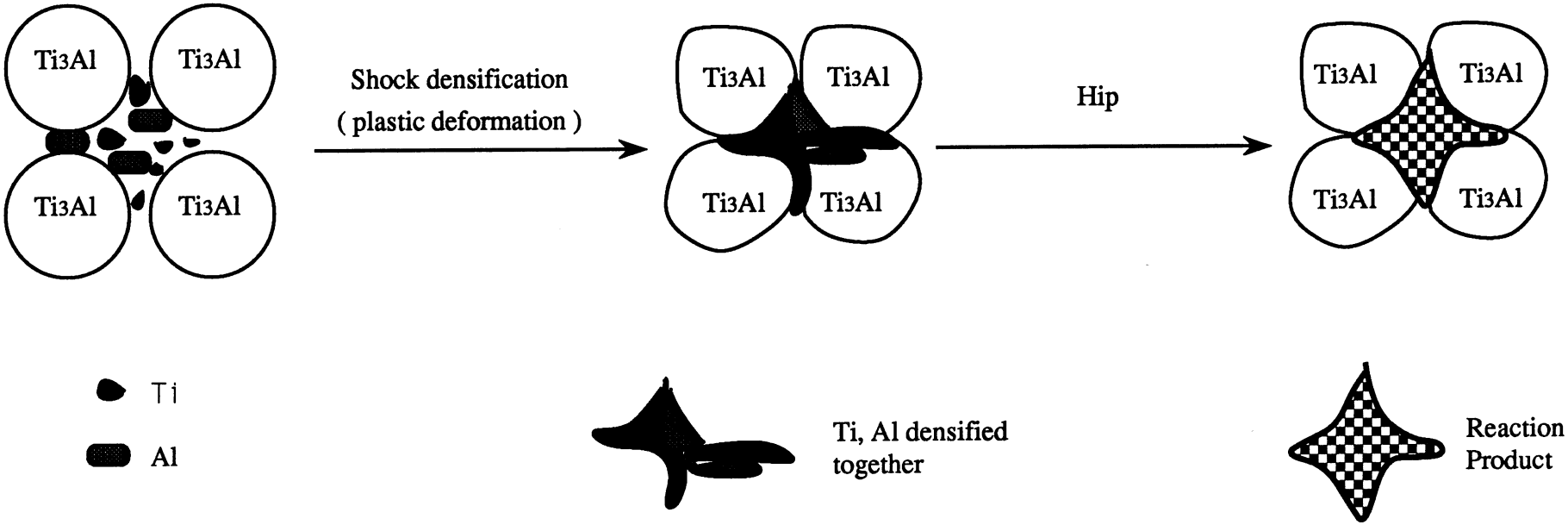

Figure 1 Schematical illustration of shock-densification and hip-induced reaction consolidation

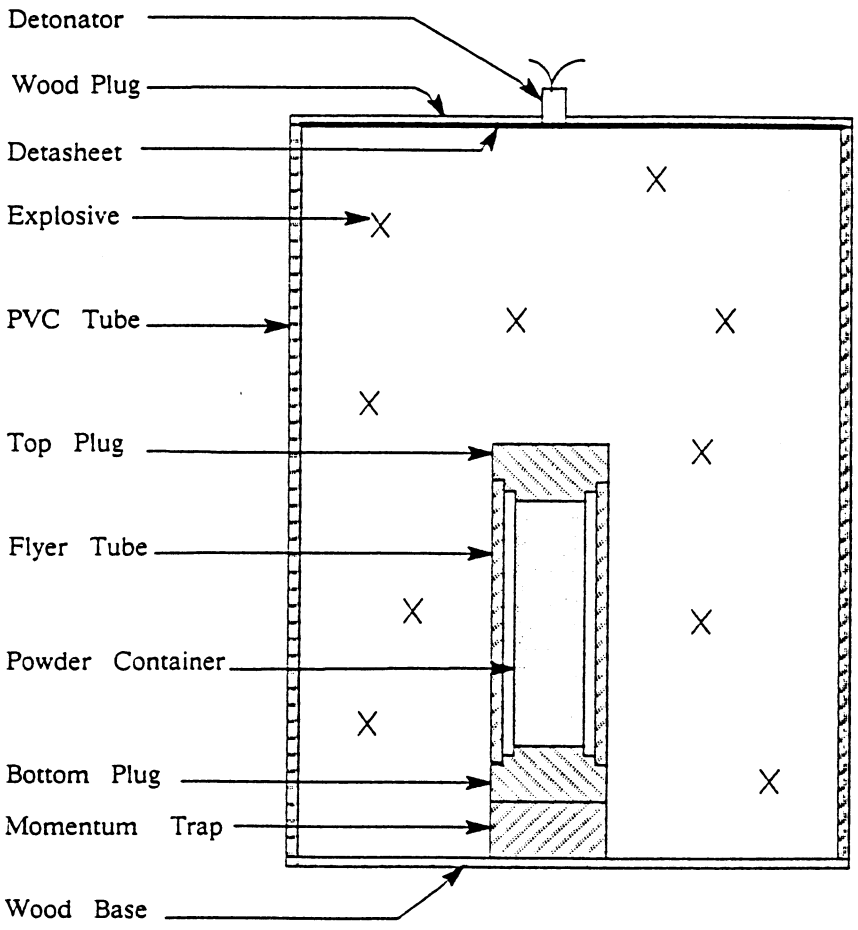

PVC Tube	
Length (mm)	635.0
O. D. (mm)	216.0
I. D. (mm)	203.0
Powder container	
Length (mm)	267.0
O. D. (mm)	38.0
I. D. (mm)	37.0
Flyer Tube	
Length (mm)	267.0
O. D. (mm)	63.0
I. D. (mm)	59.0

Figure 2 Cylindrical axisymmetric double-tube system and its experimental dimensions for cylindrical geometry.

A

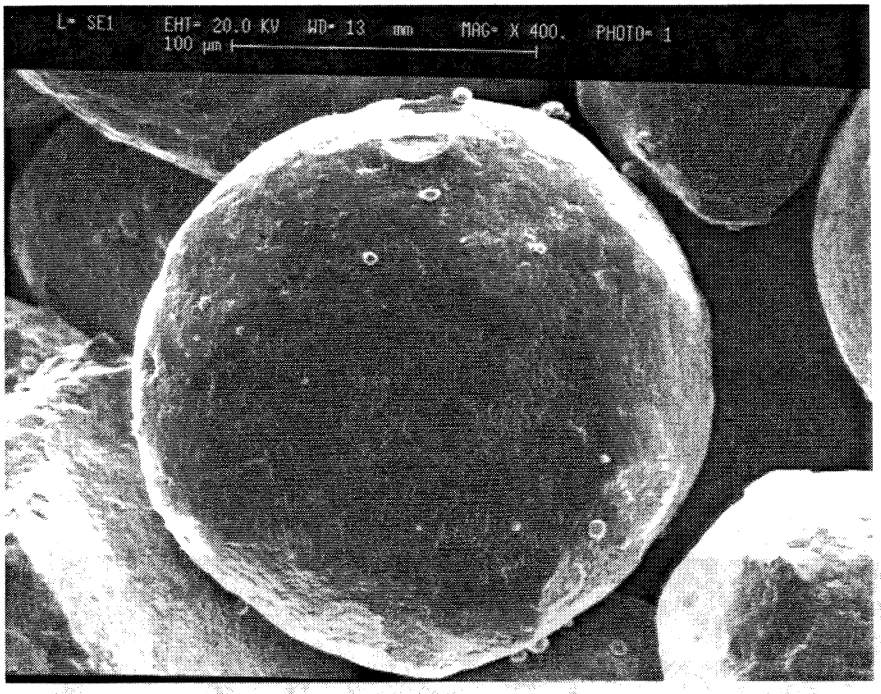

B

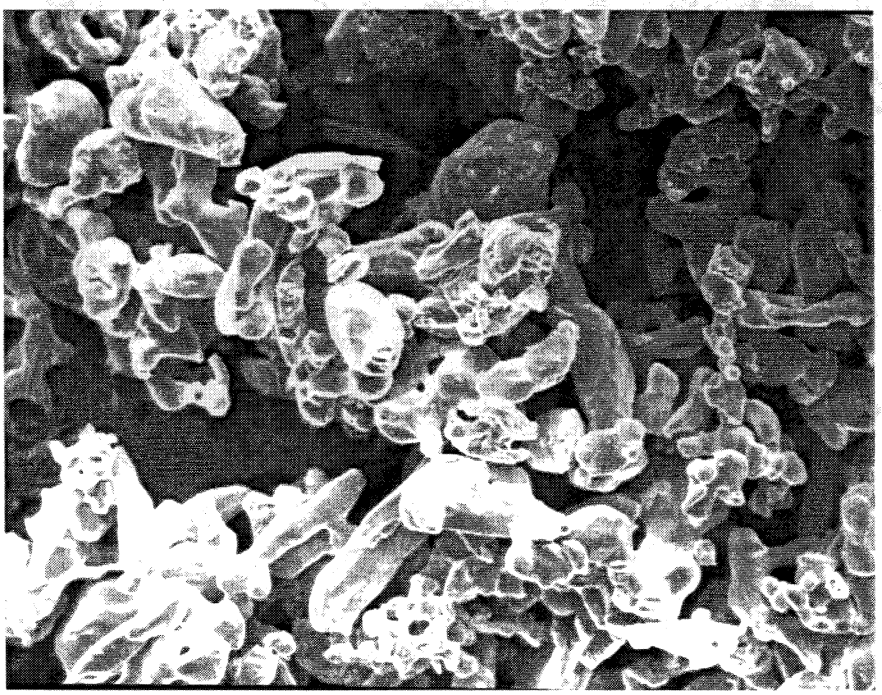

Figure 3 Scanning electron images (a) unshocked Ti_3Al powder (b) unshocked titanium having uniform alphabet size (c) unshocked aluminum.

C

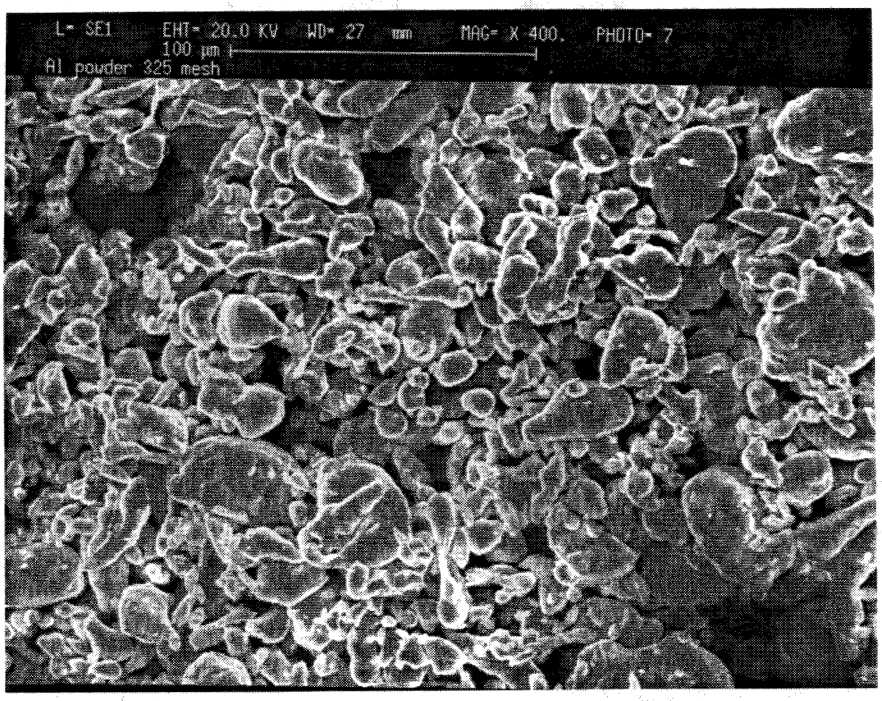
L= SE1 EHT= 20.0 KV WD= 27 mm MAG= X 400. PHOTO= 7
100 µm
Al powder 325 mesh

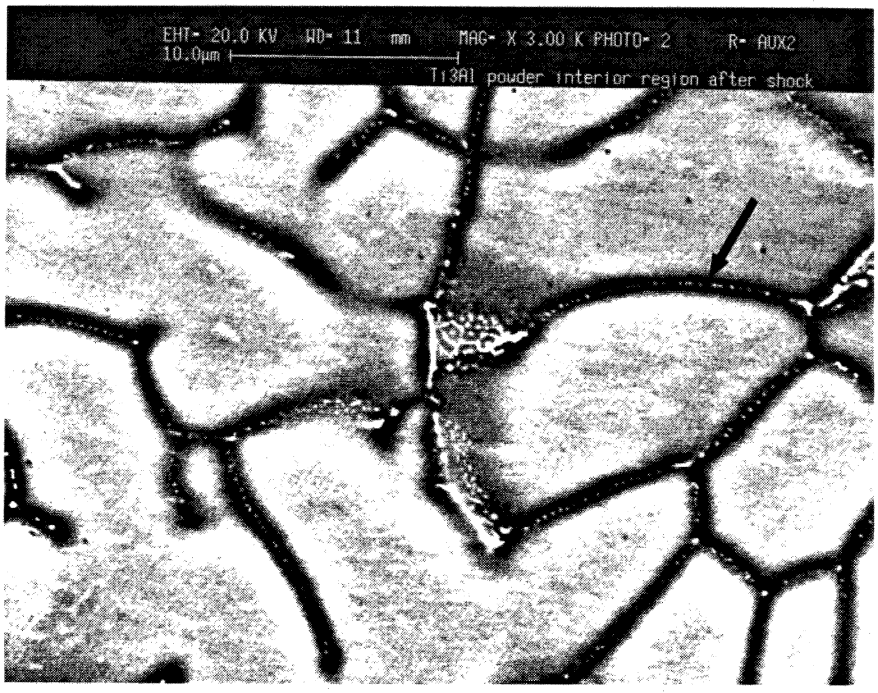

Figure 4 Scanning electron micrograph of original Ti-Al-Nb powder cross-section possessing a microcellular structure.

A

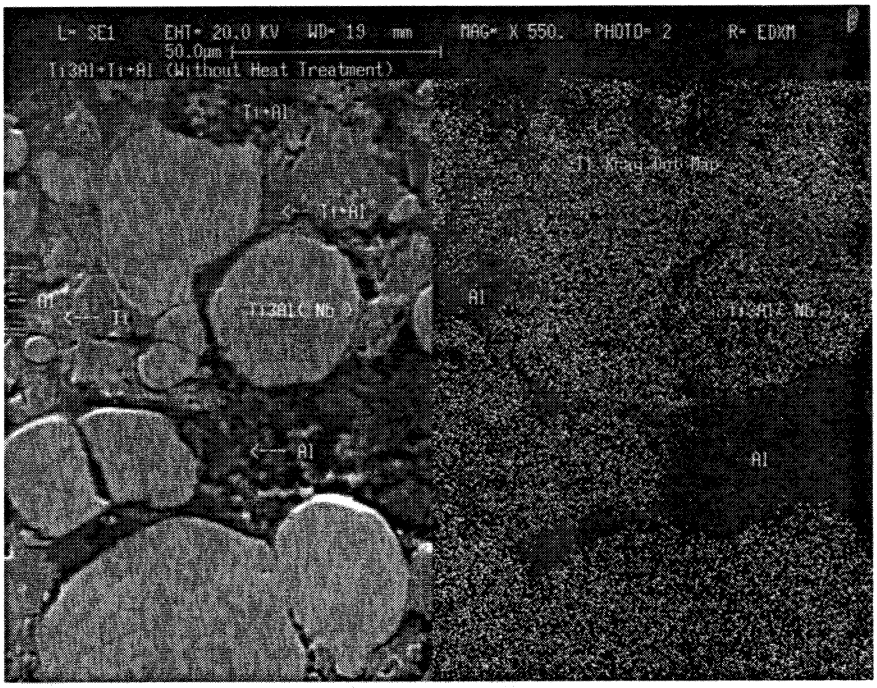

B

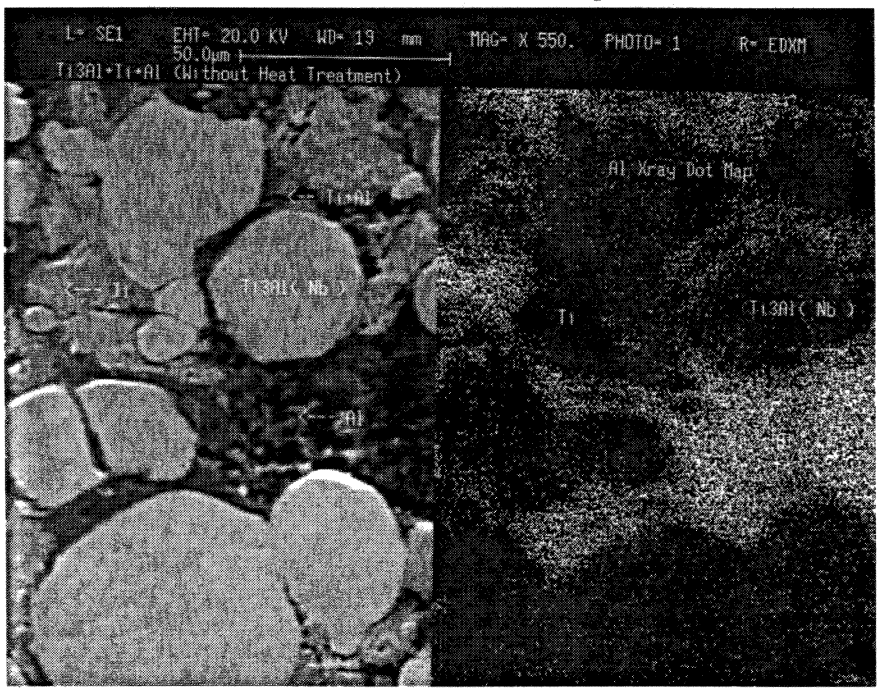

Figure 5(a) Scanning electron micrograph of shock-densified Ti_3Al +Ti + Al alloy and Ti X-ray dot mapping , and (b) Al X-ray dot mapping.

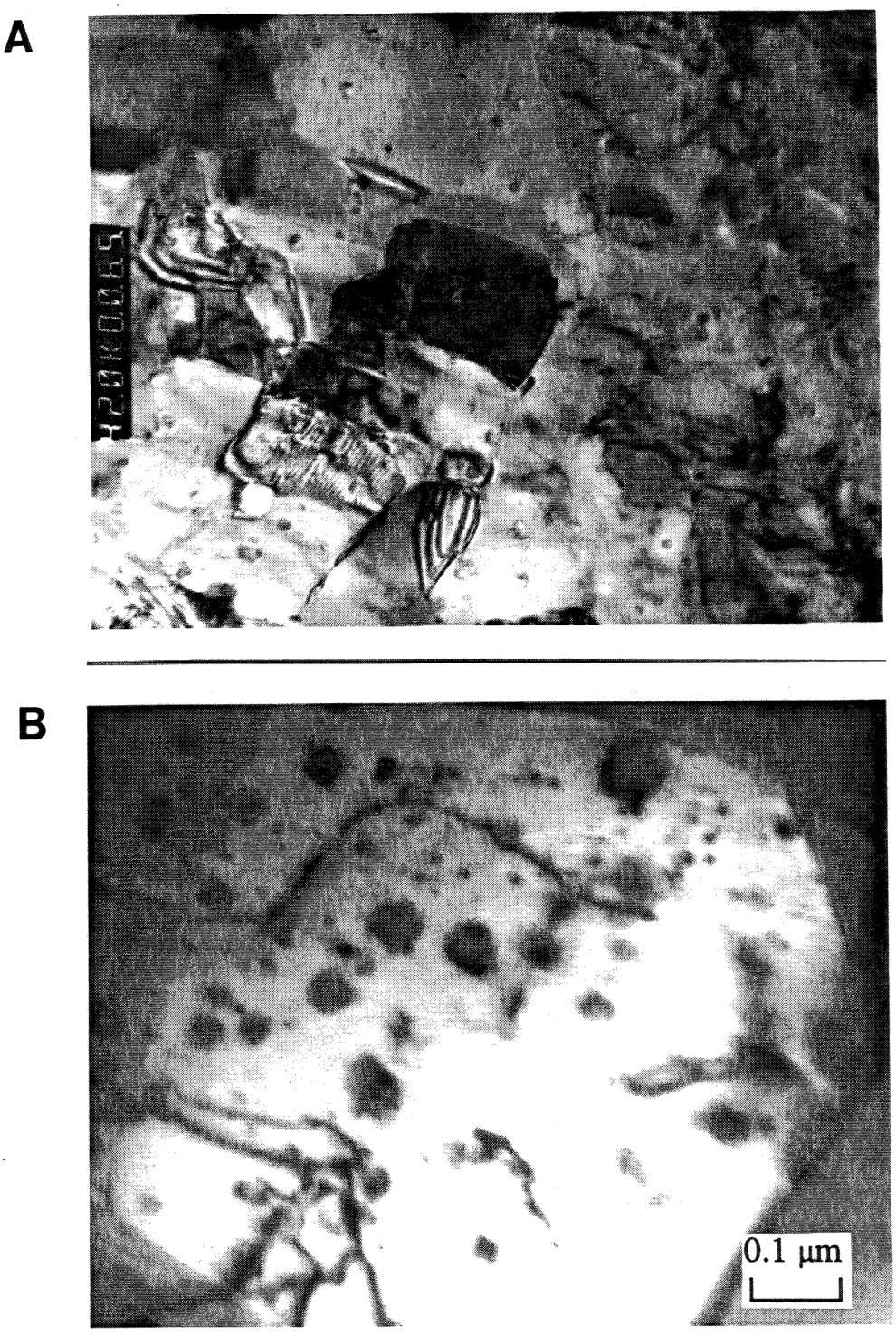

Figure 6 Bright field transmission electron micrograph from shock-densified Ti_3Al + Ti + Al alloy showing : (a) grain size approximately 500 nm , and (b) presence of dislocations and Er_2O_3 dispersoids.

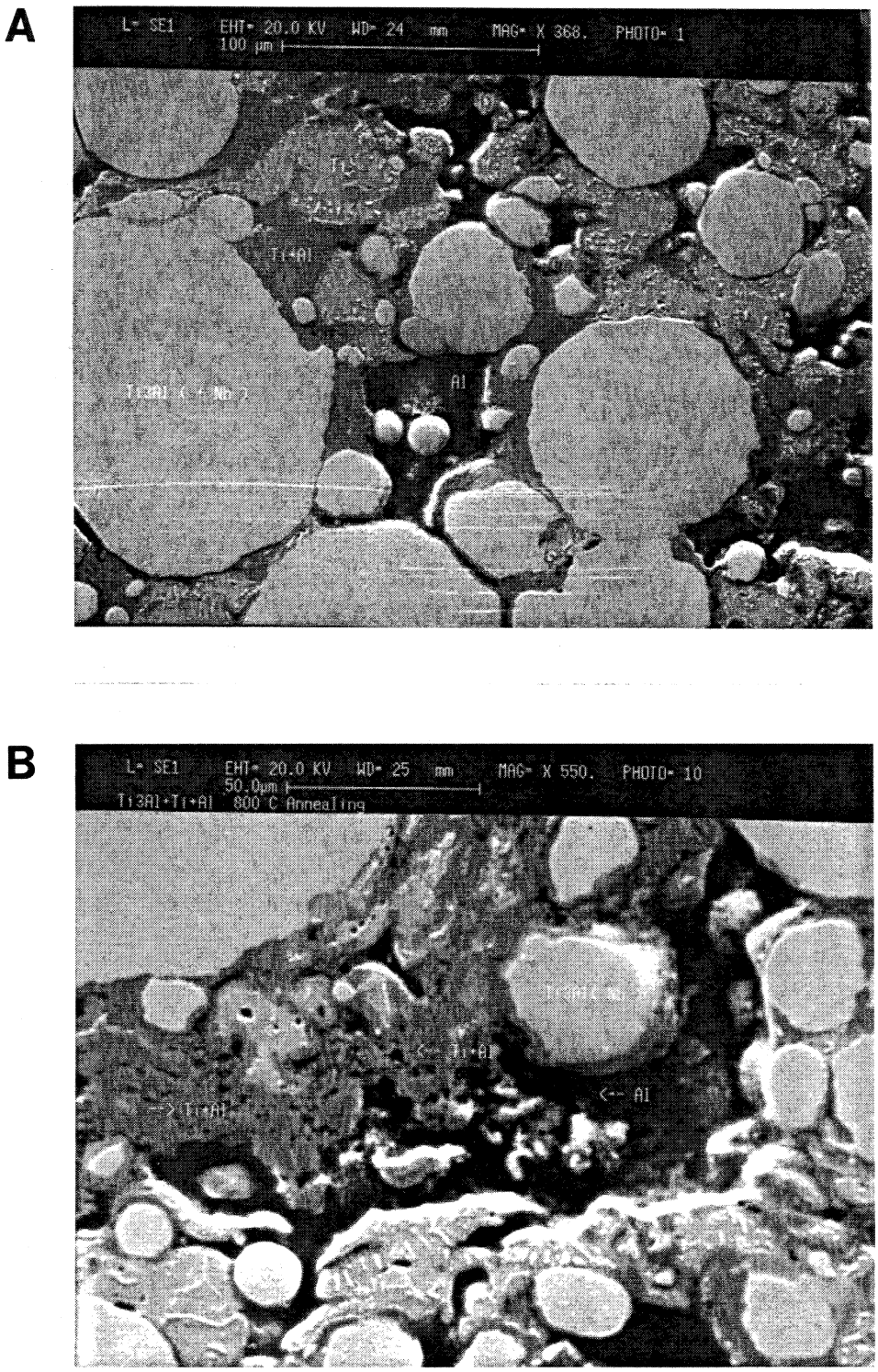

Figure 7 Scanning electron micrograph from shock-densified Ti_3Al + Ti + Al alloys (a) annealed at 600 ^{0}C (b) annealed at 800 ^{0}C in which the different regions were indetified by EDS analysis.

A

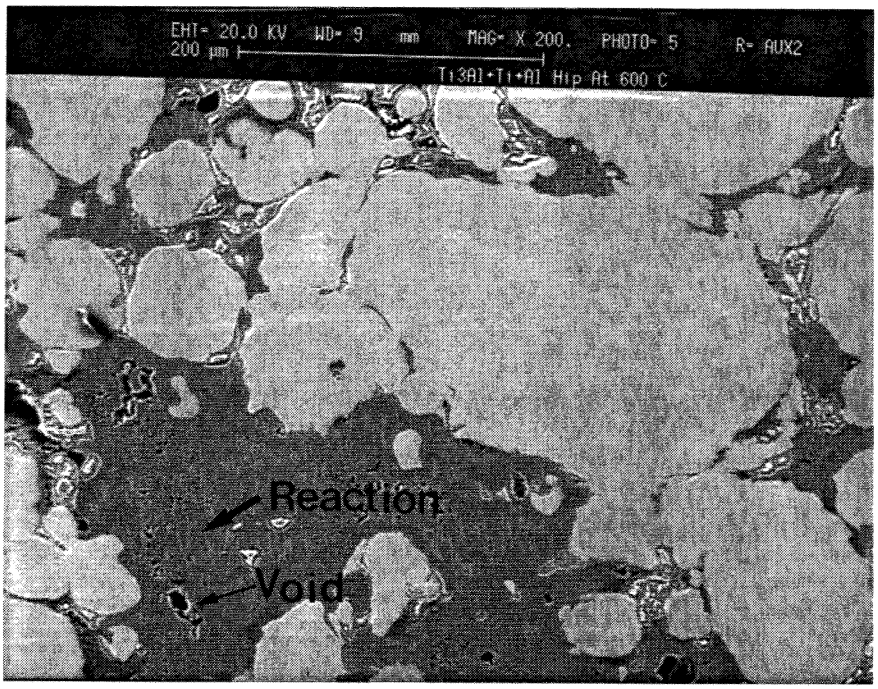

B

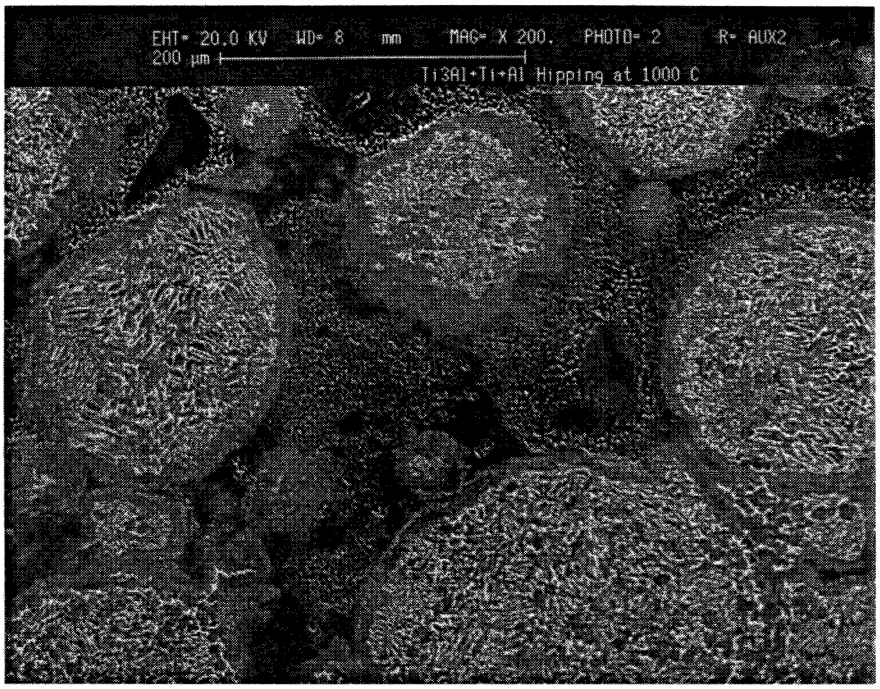

Figure 8 Scanning electron micrograph from shock-densified Ti_3Al + Ti + Al alloys (a) hipped at 600 ^{0}C (b) hipped at 1000 ^{0}C in which the different regions were indetified by EDS analysis.

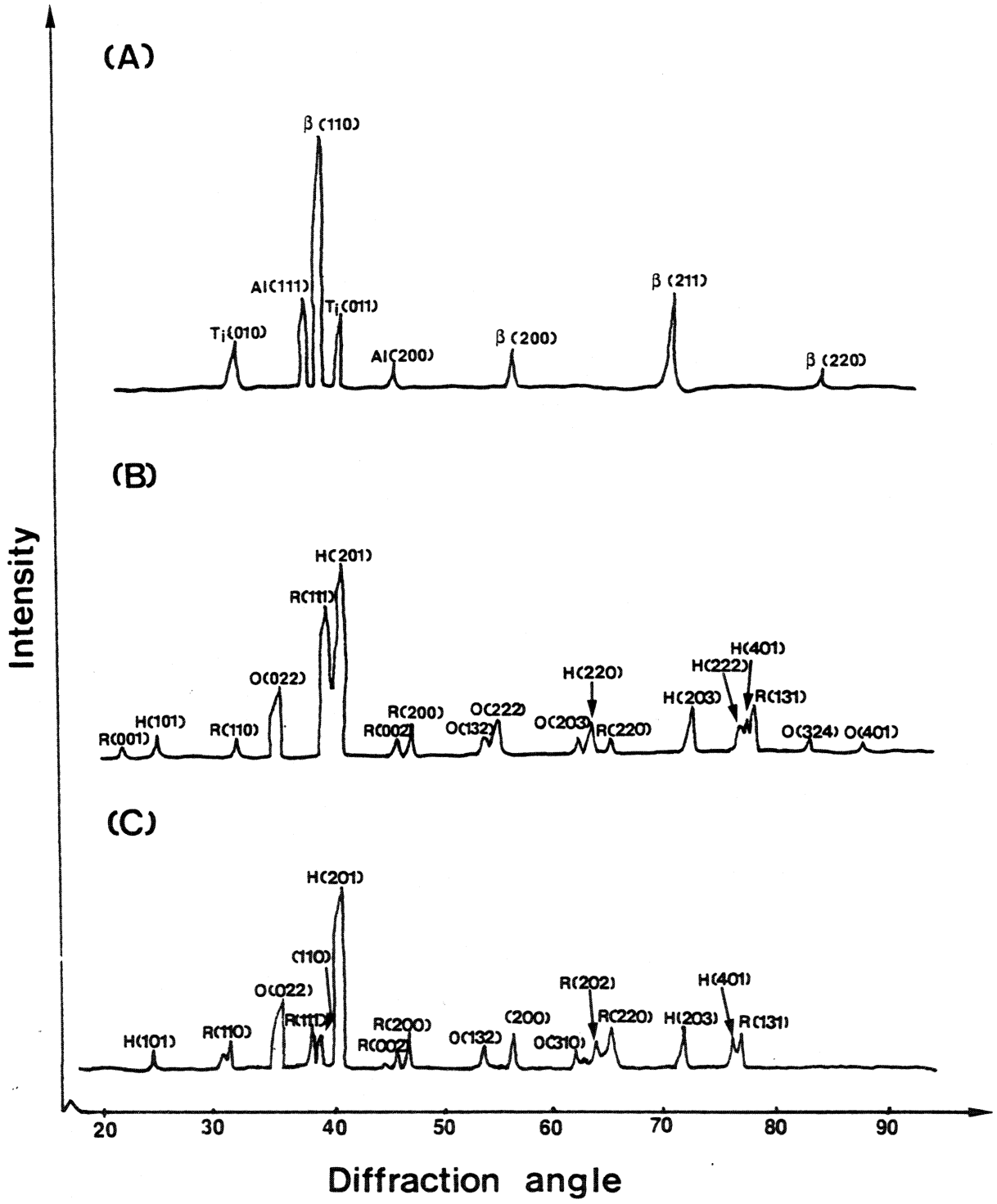

Figure 9 X-ray analysis results of as-mixed powder and compacts (a) original Ti_3Al +Ti + Al powder (b) shock-densified compacts after 600 ^{0}C hipping (c) after 1000 ^{0}C hipping

A

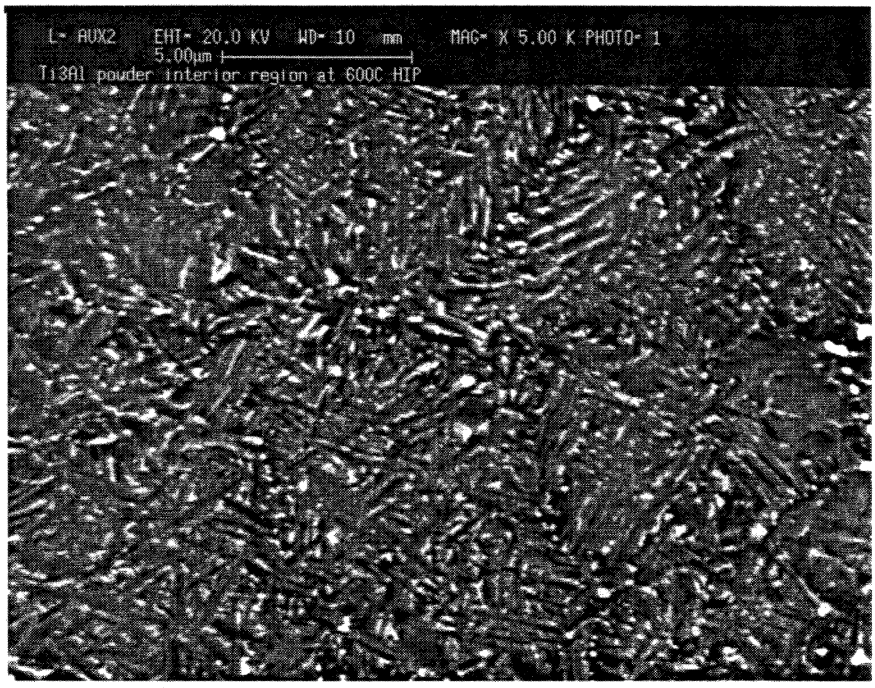

B

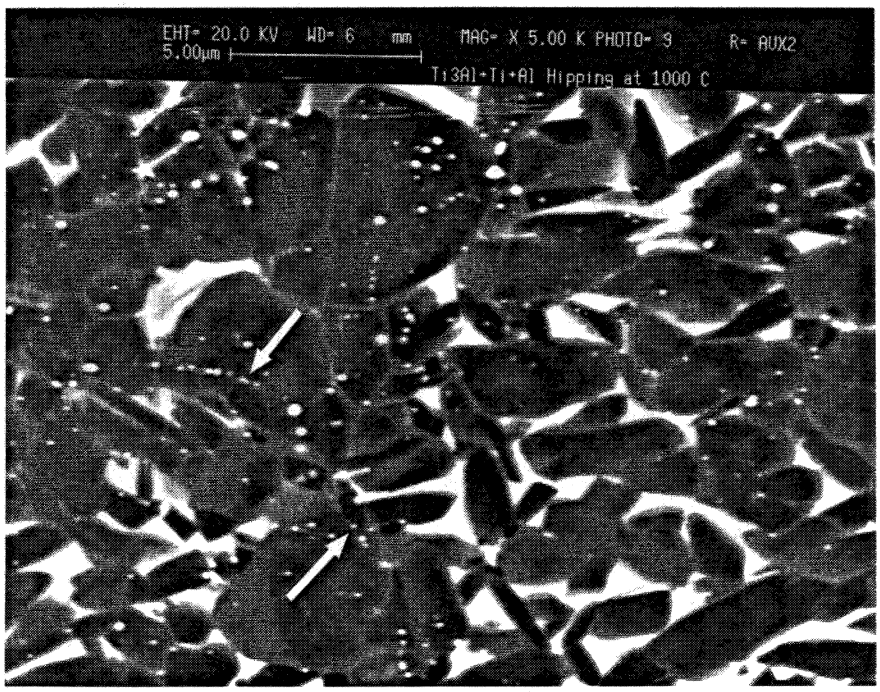

Figure 10 Scanning electron micrograph showing the microstructures of the Ti_3Al powder (a) hipped at 600 ^{0}C (b) hipped at 1000 ^{0}C.

A

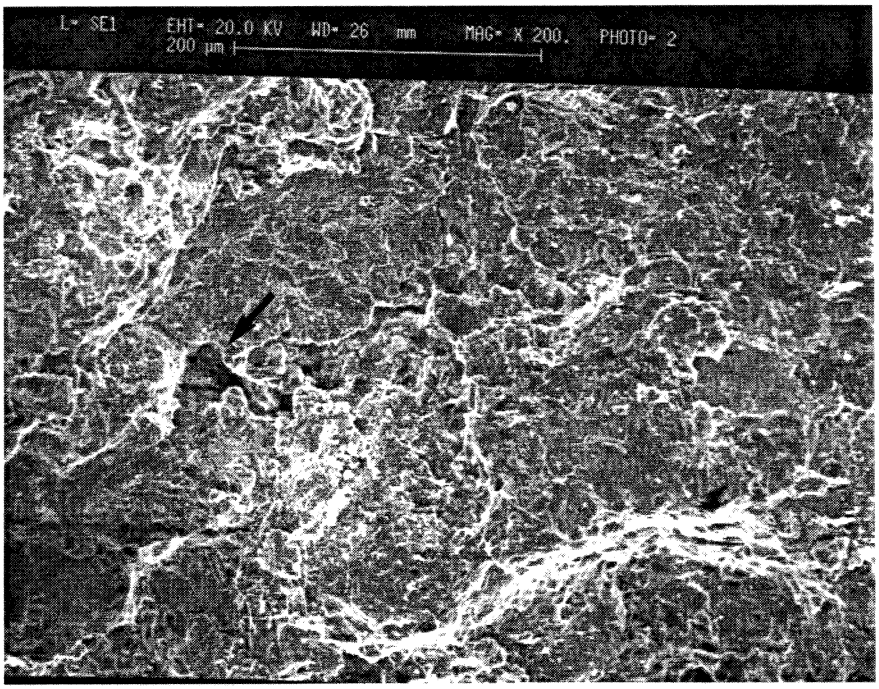

B

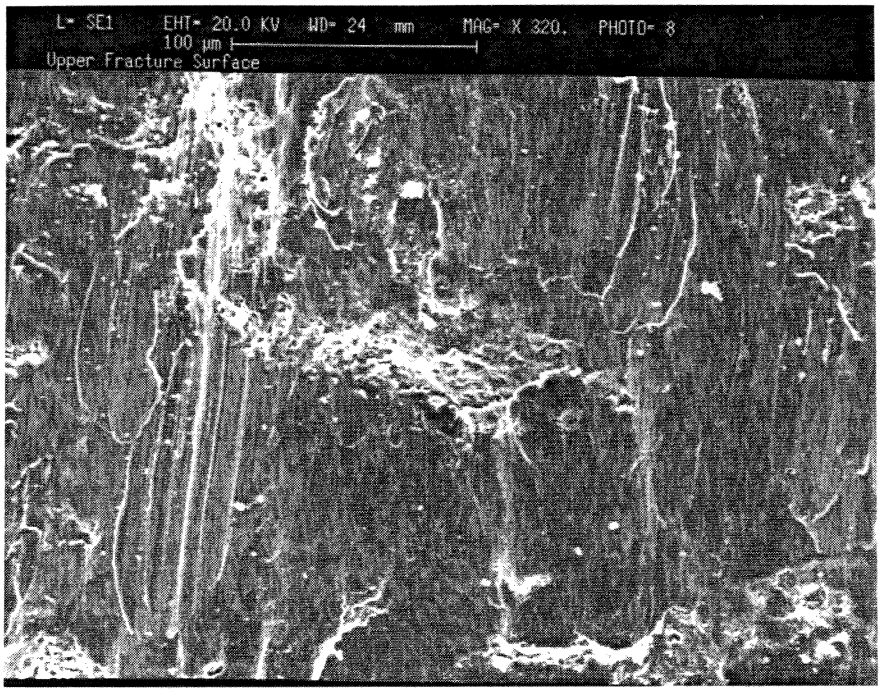

Figure 11 Fractographs from fractured surface of the 600 ^{0}C hipped specimens in compressive test : (a) lower portion which exhibited cleavage regions (b) upper portion which surfaces were smeared during shear.

A

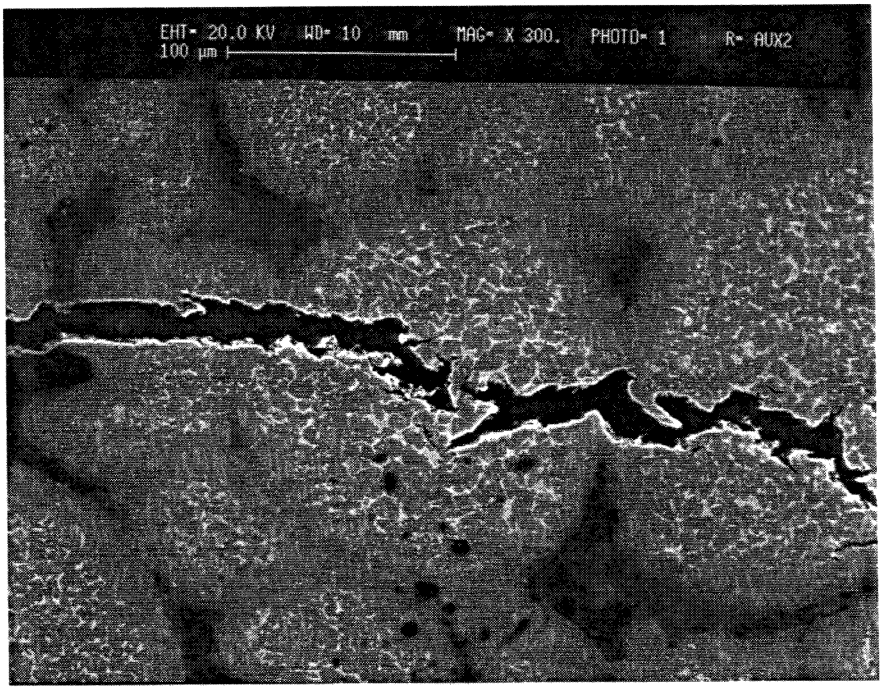

B

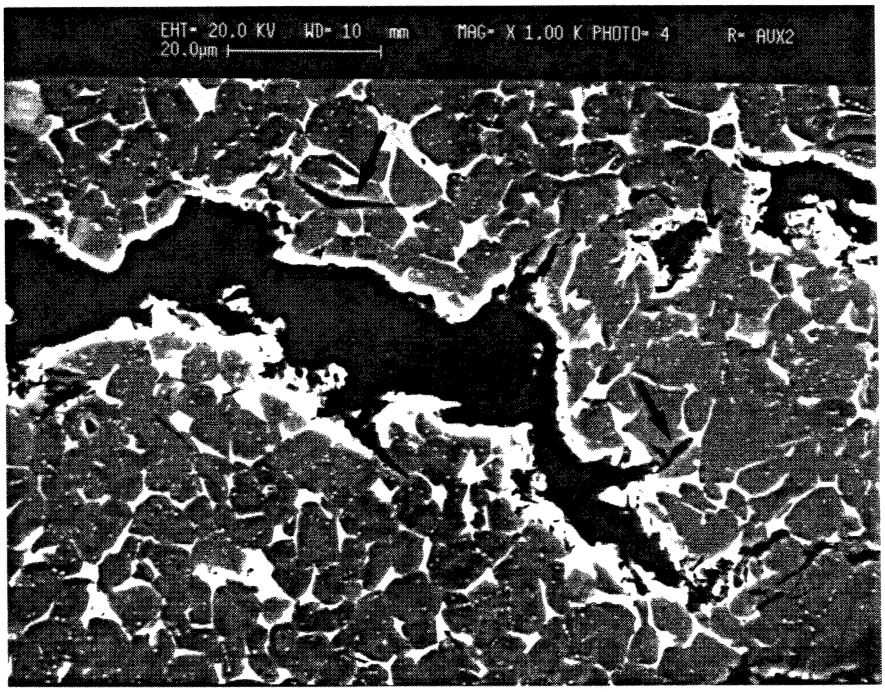

Figure 12 Scanning electron micrograph showing (a) transparticle cracks after compression test (b) intergranular and transgranular cracks in the interior of Ti_3Al particle.

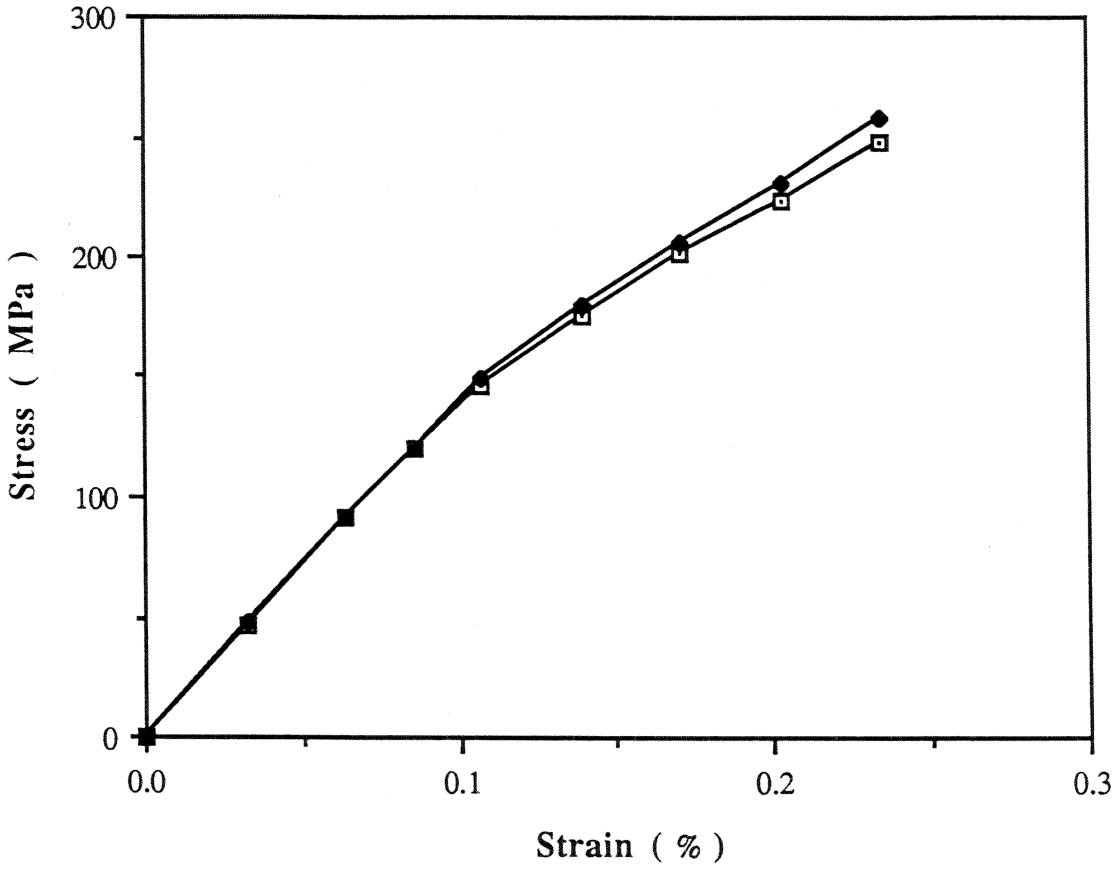

Figure 13 Stress vs strain curve of tensile test for specimens after 1000 ^{0}C hipping.

A

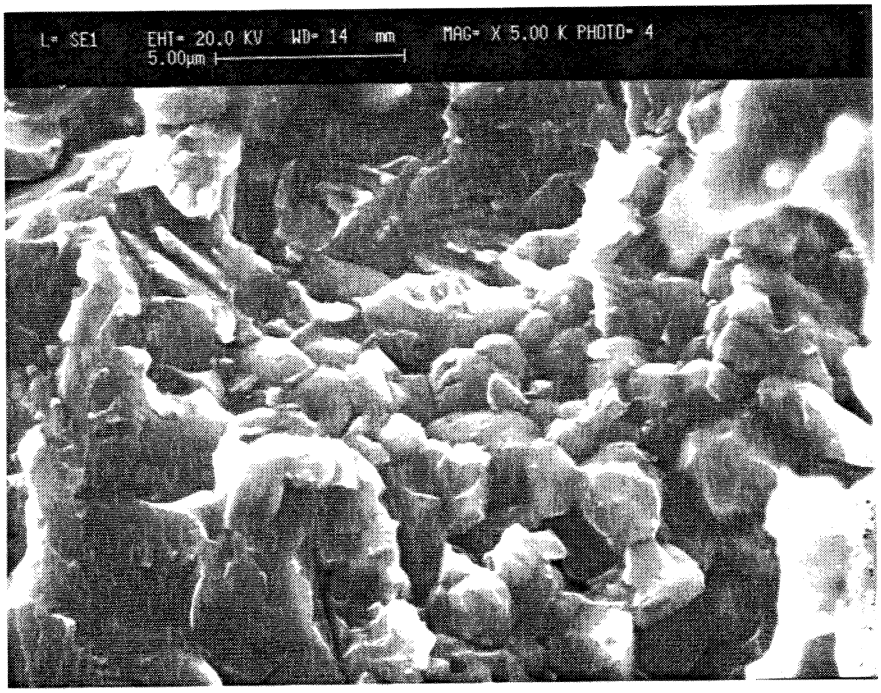

B

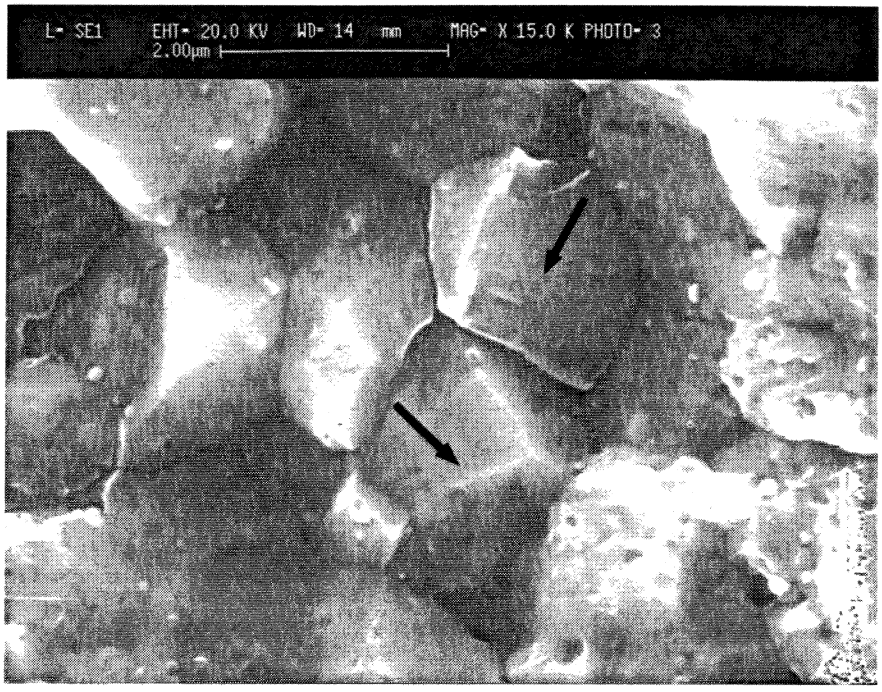

Figure 14 Fractographs from fractured surface after tensile test showing (a) intergranular cracks in the interparticle region (b) presence of dispersoids (Er_2O_3) at grain boundaries.

A

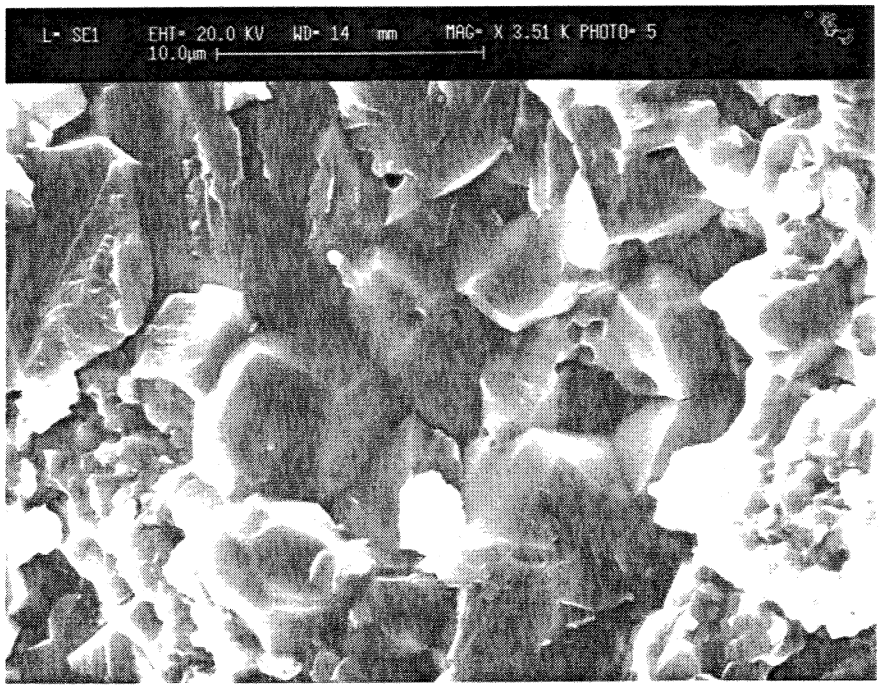

B

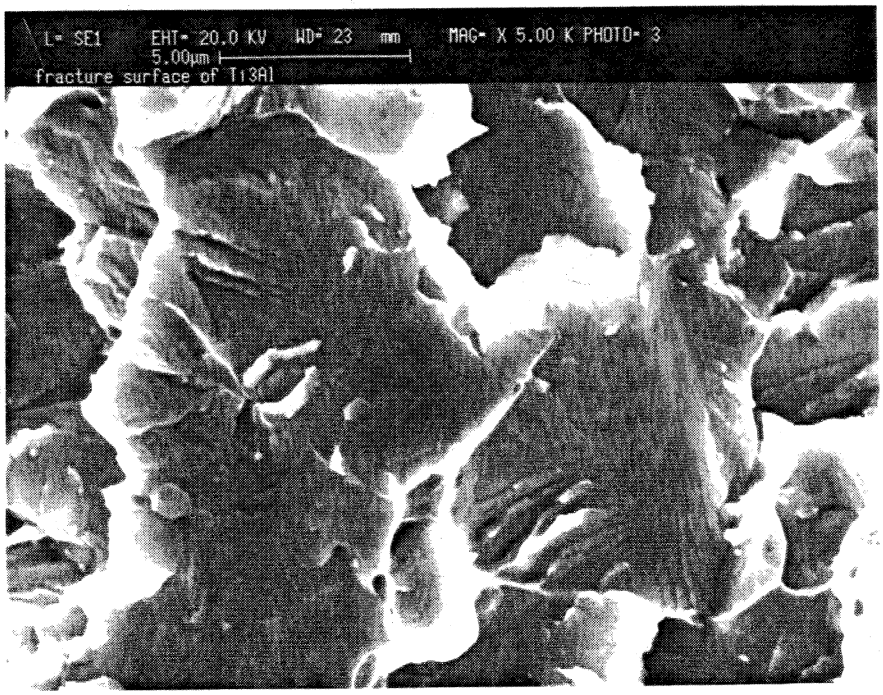

Figure 15 Scanning electron micrograph showing (a) intergranular and transgranular cracks in the Ti_3Al particle after tensile test (b) transgranular cleavage in Ti_3Al particle.

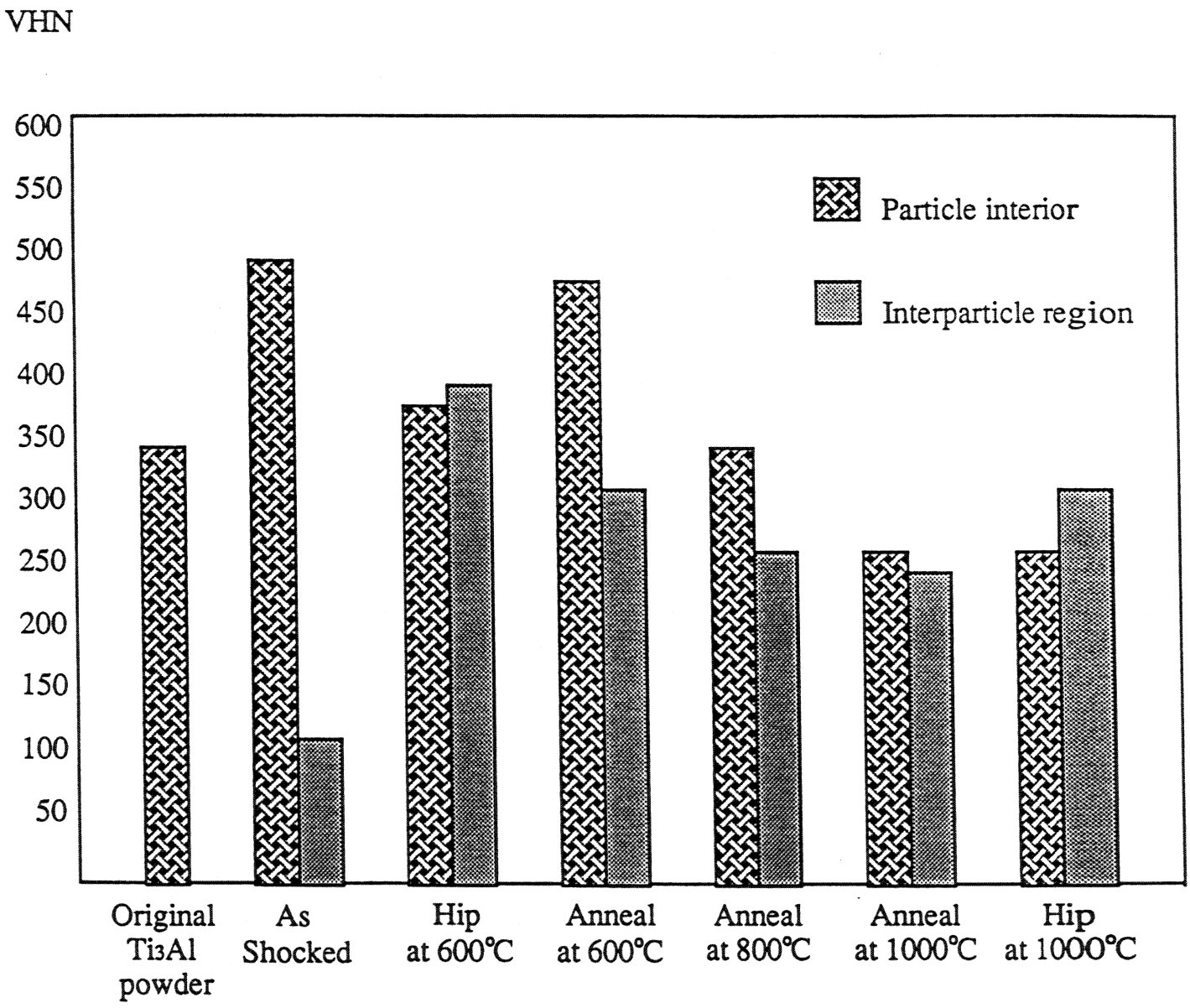

Figure 16 Microhardness values of Ti3Al hipped or annealed from 600 °C to 1000 °C